Available online at www.sciencedirect.com
SCIENCE DIRECT®
Surface Science 596 (2005) 176–186
SURFACE SCIENCE
www.elsevier.com/locate/susc

Atomic structure of the 6H–SiC(0001) nanomesh

Wei Chen [a], Hai Xu [a], Lei Liu [a], Xingyu Gao [a], Dongchen Qi [a], Guowen Peng [a], Swee Ching Tan [a], Yuanping Feng [a], Kian Ping Loh [b], Andrew Thye Shen Wee [a,*]

[a] Department of Physics, National University of Singapore, 2 Science Drive 3, Singapore 117542, Singapore
[b] Department of Chemistry, National University of Singapore, 3 Science Drive 3, Singapore 117543, Singapore

Received 10 May 2005; accepted for publication 14 September 2005
Available online 6 October 2005

Abstract

The atomic structure of the carbon nanomesh template (the so-called $6\sqrt{3} \times 6\sqrt{3}R30^\circ$ reconstruction) on the 6H–SiC(0001) surface was investigated in detail by scanning tunneling microscopy (STM), low energy electron diffraction (LEED), synchrotron photoemission spectroscopy (PES) and density-functional theory (DFT) calculations. We propose that the origin of the carbon nanomesh template arises from the self-organization of excess carbon atoms forming a novel honeycomb arrangement atop the 6H–SiC(0001) surface after annealing at 1100 °C. Two carbon nanomesh-related C 1s components are observed at binding energies of 285.1 eV (S_1) and 283.8 eV (S_2) by angle-resolved synchrotron PES experiments. We assign the S_2 component to carbon atoms that bond to one underlying Si atom, and the S_1 component to carbon atoms bonded to other carbon atoms without Si–C bond formation. Further annealing results in the formation of crystalline graphitic layers on top of the surface.

Keywords: STM; Nanomesh; Self-organization

1. Introduction

Recently, intense efforts have focused on the fabrication of two-dimensional self-assembled nanotemplates that have preferential sites that accommodate individual nanostructures favoring the formation of well-ordered nanometer-sized functional arrays [1–10]. For example, supramolecular networks stabilized by selective non-covalent bonds have been used as templates to form C_{60} honeycomb superstructures [9]; strain–relief patterns generated by the deposition of material with a different lattice constant to that of the substrate result in the formation of well-ordered

* Corresponding author. Tel.: +65 68746362; fax: +65 67776126.
E-mail address: phyweets@nus.edu.sg (A.T.S. Wee).

0039-6028/$ - see front matter © 2005 Elsevier B.V. All rights reserved.
doi:10.1016/j.susc.2005.09.013

2D arrays of nanostructures [1,10]. In particular, an interesting nanotemplate of $6\sqrt{3} \times 6\sqrt{3}R30^\circ$ reconstruction on 6H–SiC (0 0 0 1) has been observed, resembling a honeycomb structure with unit cells with diameter of about 2 nm [11–24]. This nanotemplate has promising potential for the growth of size-controlled metal clusters. For example, we have reported that this nanotemplate can be used as a chemically inert nanotemplate for the preparation of cobalt (Co) nanoparticles [11,12]. It is also effective in isolating the Co nanoclusters, favoring the formation of monodispersed Co nanoclusters with a narrow size distribution.

However, the atomic structure of the surface is still not well understood. In the literature, the $6\sqrt{3} \times 6\sqrt{3}R30^\circ$ reconstruction on 6H–SiC (0 0 0 1) or on the closely-related 3C–SiC(1 1 1) surface displays a $6\sqrt{3} \times 6\sqrt{3}R30^\circ$ LEED diffraction pattern; while in the STM images, it shows an incommensurate "6×6" honeycomb superstructure [13–27]. Although some researchers argue that the "$6\sqrt{3} \times 6\sqrt{3}R30^\circ$" notation for the LEED pattern is incorrect, they continue to refer to this structure as "$6\sqrt{3} \times 6\sqrt{3}R30^\circ$" for consistency [18]. Some researchers suggested that the formation of this reconstruction may be due to a layer of graphite resting above the $\sqrt{3} \times \sqrt{3}R30^\circ$ array of Si adatoms [16,17] or on the SiC bulk 1×1 plane [13–15]. However, Johansson and Owman demonstrated that the graphite layer only formed at a temperature higher than that required for a well-developed $6\sqrt{3} \times 6\sqrt{3}R30^\circ$ reconstruction in a high resolution core-level PES study [19] and combined STM and LEED experiments [18]. In our previous STM studies, this surface did not always retain "6×6" periodicity. For example, the pore size of some honeycombs could be effectively enlarged after prolonged annealing at 1100 °C: the diameter could be enlarged from 20.0 ± 2.0 Å to 25.0 ± 2.0 Å, and the apparent height from 1.5 ± 0.1 Å to 3.2 ± 0.1 Å [12]. As such, this surface can be described as a dynamic superstructure formed by the self-organization of surface carbon atoms at high temperature, and we referred to it as a "carbon nanomesh" [12]. In this paper, we continue to use this notation of "carbon nanomesh" instead of the "$6\sqrt{3} \times 6\sqrt{3}R30^\circ$ reconstruction" to avoid confusion. The aim of this paper is to elucidate the detailed surface structure of the carbon nanomesh, in order to attain precise control of the fabrication of well-ordered functional nanostructures using this template. The atomic structure of the carbon nanomesh is investigated in detail by STM, LEED, synchrotron photoemission experiments, and density-functional theory (DFT) calculations.

2. Experimental

The STM experiments were carried out in a multichamber UHV system with a base pressure of 1×10^{-10} Torr, allowing in situ transfer between facilities for surface analytical techniques available including variable temperature scanning tunneling microscopy (Omicron VT-STM), X-ray photoelectron spectroscopy (XPS), and low energy electron diffraction (LEED) [11,12,20]. A Si-terminated n-type 6H–SiC(0 0 0 1) sample (CREE Research Inc.) was first annealed at 850 °C under a silicon flux for 2 min, resulting in a Si-rich 3×3-reconstructed surface [28]. The sample was then annealed several times at 1100 °C in the absence of the silicon flux to form the carbon nanomesh [11,12]. Synchrotron photoemission experiments were performed in a UHV chamber with base pressure of 5×10^{-11} Torr at the SINS beamline of the Singapore Synchrotron Light Source (SSLS) [47]. The chamber is equipped with an AFM/STM (Omicron) and LEED for in situ characterization. Photoemission spectroscopy (PES) was performed using p-polarized light with photon energy resolution $E/\Delta E$ set at about 1000, and a hemispherical electron energy analyzer (EA 125, Omicron Nano-Technology GmbH.).

3. Results and discussion

The carbon nanomesh was formed by annealing the n-type 6H–SiC (0 0 0 1) surface at 1100 °C for 5 min. The STM filled state images of this carbon nanomesh at different tip biases are shown in Fig. 1(a)–(d). The tunneling current was fixed at 0.2 nA and the tip bias was varied from 1.5 V to

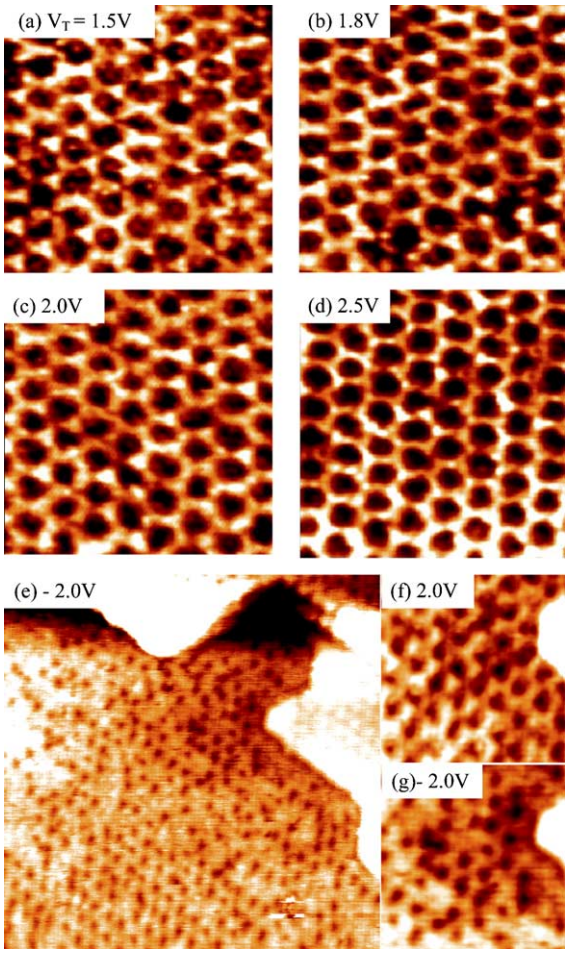

Fig. 1. 20×20 nm^2 STM filled state images of the carbon nanomesh at different bias: (a) $V_T = 2.5$ V, (b) $V_T = 2.0$ V, (c) $V_T = 1.8$ V, (d) $V_T = 1.5$ V, (e) 50×50 nm^2 STM empty state image at bias of $V_T = -2.0$ V. 17×17 nm^2 STM images with reverse bias polarity at the same region: (f) $V_T = 2.0$ V and (g) $V_T = -2.0$ V.

2.5 V. As shown in Fig. 1, this nanomesh surface comprises incommensurate honeycombs with periodicity close to 6×6. Most honeycombs have diameters of 20.0 ± 2.0 Å, close to "6×6" periodicity of SiC 1×1 (around 19 Å), and the apparent height of 1.5 ± 0.1 Å as determined from the line profiles of the STM images. Fig. 1(e) shows the 50×50 nm^2 STM empty state image of the carbon nanomesh surface ($V_T = -2.0$ V), which clearly displays the honeycomb structures. The comparison of STM images at the same region with reverse bias polarity (Fig. 1(f): $V_T = 2.0$ V; Fig. 1(g): $V_T = -2.0$ V) indicates that the structure of the carbon nanomesh is real, and not of electronic origin as observed on the recently reported electronic Moirè patterns on lead (Pb) quantum islands [29]. As reported in our previous study, the pore size of the honeycombs on the carbon nanomesh surface could be enlarged by annealing the SiC substrate at 1100 °C for a longer time (about 20 min) [12]. Fig. 2(a) shows the 150×150 nm^2 STM filled state image of the carbon nanomesh surface prepared by prolonged annealing. Fig. 2(b) is the corresponding detailed 43×43 nm^2 STM image. A comparison of the line profiles across the honeycombs after short (Fig. 1(d)) and prolonged annealing (Fig. 2(b)) is presented in Fig. 2(c). It can be clearly seen that the pore diameter of the honeycombs after prolonged annealing was enlarged to 25.0 ± 2.0 Å, and the apparent height increased to 3.2 ± 0.1 Å. Short annealing (1100 °C for 5 min) results in a nanomesh comprising honeycombs with 6×6 periodicity as shown in Fig. 1, but prolonged annealing results in the distortion of the honeycombs as shown in Fig. 2(b). As such, we deduce that this carbon nanomesh is a superstructure formed by the self-organization of carbon atoms at high temperature, and the size of the honeycombs can be changed by prolonged annealing.

Fig. 3 shows the LEED patterns (left panel) and corresponding STM filled state images (right panel) of the SiC surface after annealing at different temperatures. After annealing at 1050 °C for 5 min (Fig. 3(a)), the STM image clearly shows the coexistence of two structures: the upper region shows the disordered $\sqrt{3} \times \sqrt{3}R30^\circ$ reconstruction and the lower region shows the carbon nanomesh pattern. Hereafter, we refer to this surface as the "$\sqrt{3} \times \sqrt{3}R30^\circ$ + carbon nanomesh mixed surface". The corresponding LEED pattern of this surface as displayed in the left panel of Fig. 3(a), was previously referred to as the "$6\sqrt{3} \times 6\sqrt{3}R30^\circ$" LEED pattern by van Bommel et al. [30], and subsequently by several others [13–17]. The white circles in the LEED pattern of Fig. 3(a) highlight the $\sqrt{3} \times \sqrt{3}R30^\circ$ LEED diffraction spots. This surface was further annealed at 1100 °C for 5 min. At this stage, the $\sqrt{3} \times \sqrt{3}R30^\circ$ reconstruction vanishes

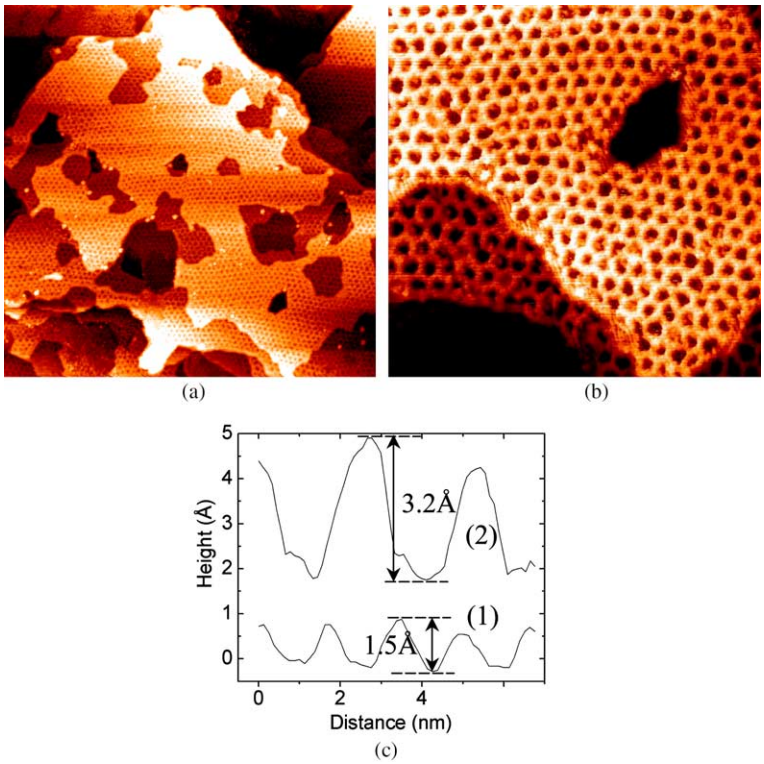

Fig. 2. (a) $150 \times 150\ nm^2$ and (b) corresponding detailed $43 \times 43\ nm^2$ STM filled state images of the SiC honeycomb template after prolonged annealing at 1100 °C for 20 min. $V_T = 2.5$ V, $I = 0.2$ nA. (c) Line profiles of the carbon nanomesh surface prepared by annealing at 1100 °C for 5 min [line (1)] and of that prepared after prolonged annealing at 1100 °C for 20 min [line (2)].

from the STM image (Fig. 3(b)), and the surface was fully covered by the incommensurate honeycomb-like nanomesh structure with approximate 6×6 periodicity. The LEED pattern in Fig. 3(b) clearly shows the disappearance of the $\sqrt{3} \times \sqrt{3}R30°$ diffraction spots as compared to Fig. 3(a). Therefore, we refer to this surface as the "pure carbon nanomesh surface". These results are consistent with Owman's observation by STM and LEED [18].

The C 1s core-level spectra for the $\sqrt{3} \times \sqrt{3}R30°$ surface after subsequent heat treatments are shown in Fig. 4. To increase the surface sensitivity, a photon energy of 350 eV and an emission angle of 40° were used, giving an electron escape depth of about 2.6 Å [31]. First, the 3×3 surface was prepared by annealing the SiC substrate at 850 °C under silicon flux for 2 min. The 3×3 reconstruction was confirmed by LEED and STM. The surface was then annealed at 950 °C for 5 min in the absence of Si flux and a sharp $\sqrt{3} \times \sqrt{3}R30°$ LEED diffraction pattern was formed. The C 1s core-level spectrum (Fig. 4(a)) is dominated by the bulk SiC peak at a binding energy of 282.9 eV. The $\sqrt{3} \times \sqrt{3}R30°$ surface was free of oxygen and other contamination, as determined by the wide scan PES spectrum using a photon energy of 700 eV (not shown here). Further annealing at 1050 °C for 5 min led to the formation of a "$\sqrt{3} \times \sqrt{3}R30° +$ carbon nanomesh mixed surface" as described previously. A new component peak at 285.1 eV appears in the C 1s spectrum in Fig. 4(b). The "pure carbon nanomesh surface" was formed after annealing the SiC substrate at 1100 °C for 5 min. At this stage, the 285.1 eV peak dominates the C 1s spectrum (Fig. 4(c)) accompanied by a shoulder at 238.8 eV; the bulk-related SiC component at 282.9 eV is almost gone. After

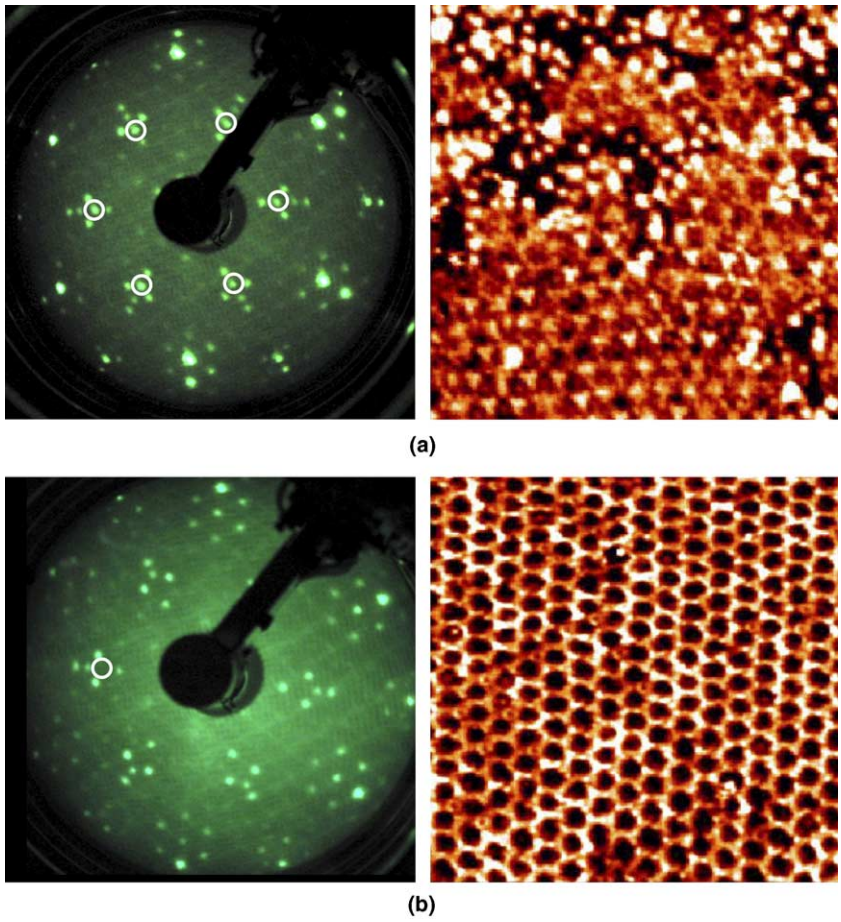

Fig. 3. LEED patterns (left) and corresponding 30×30 nm^2 filled state STM images (right) of (a) "$\sqrt{3} \times \sqrt{3}R30^\circ$ + carbon nanomesh mixed surface" and (b) "well-developed carbon nanomesh surface" on 6H–SiC(0001). LEED incident beam energy: 70 eV, $V_T = 2.5$ V, $I = 0.2$ nA. The white circles highlight the $\sqrt{3} \times \sqrt{3}R30^\circ$ LEED spots.

further annealing at 1200 °C for 5 min, the C 1s spectrum (Fig. 4(d)) broadens to the lower binding energy side, and a new component peak at 284.4 eV is just resolvable. A freshly cleaved highly ordered pyrolytic graphite (HOPG) sample was used as the reference sample, and the binding energy of the C 1s from HOPG was found to be 284.5 eV. Hence, we attribute this new component peak at 284.4 eV to the crystalline graphite layers formed at this temperature, and the surface is named "nanomesh + graphite mixed surface". Annealing at 1300 °C for 5 min gives a C 1s spectrum dominated by the signal from the graphite layer (Fig. 4(e)). Hence, graphitization of the SiC surface only occurs at temperatures higher than that required for the formation of the "pure carbon nanomesh surface". The results clearly distinguish the carbon nanomesh surface and graphitization of the SiC surface, consistent with Johansson's high resolution PES findings [19]. The graphitization of the SiC surface at certain high temperature is accompanied by the evaporation of silicon atoms from the bulk, and is not due to the same mechanism of the carbon graphitization on transition metal surfaces [32,33].

Angle-resolved photoemission spectra (a photon energy at 350 eV) taken at emission angles of 40° and 90° (normal to the surface and less surface

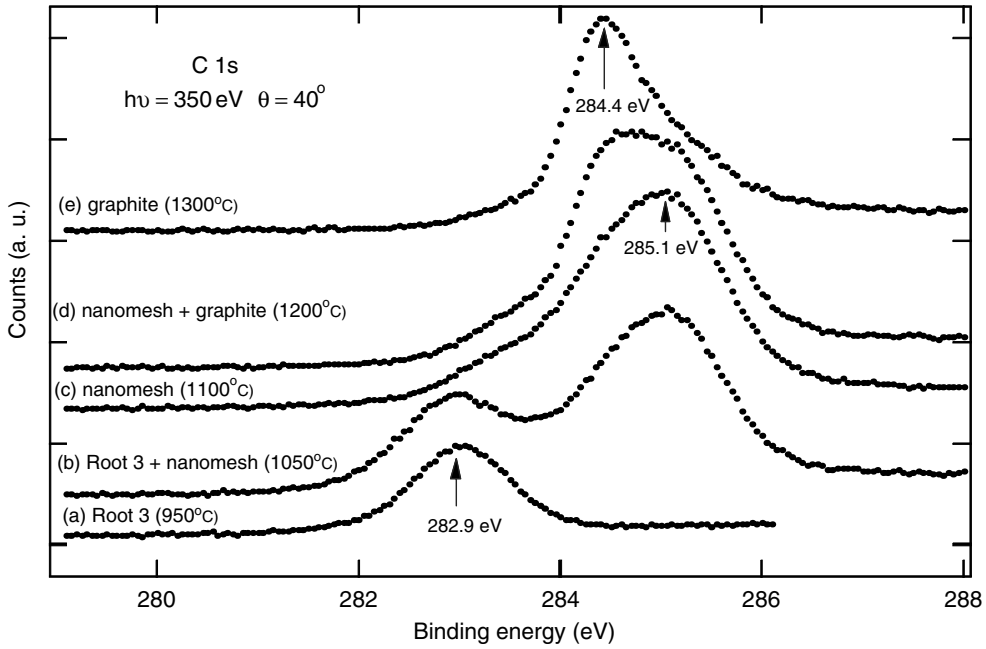

Fig. 4. C 1s core-level spectra recorded from the $\sqrt{3} \times \sqrt{3}R30^\circ$ surface and after different heat treatments, measured at a photon energy of 350 eV and an emission angle of 40°. (a) $\sqrt{3} \times \sqrt{3}R30^\circ$ surface, (b) $\sqrt{3} \times \sqrt{3}R30^\circ$ + carbon nanomesh mixed surface, (c) pure carbon nanomesh surface, (d) carbon nanomesh + graphite mixed surface and (e) graphite surface.

sensitive) were used to identify surface or bulk-related components on the carbon nanomesh surface. The C 1s spectra of the "$\sqrt{3} \times \sqrt{3}R30^\circ$ + carbon nanomesh mixed surface" recorded at two emission angles of 90° and 40° are shown in Fig. 5. At the more surface sensitive emission angle of 40°, the intensity of the 285.1 eV component is stronger than that at 282.9 eV. However, at the less surface sensitive emission angle of 90°, the intensity of the 285.1 eV component is weaker than that at 282.9 eV. Therefore, the 282.9 eV component is attributed to the bulk-related SiC, and the 285.1 eV component to the carbon nanomesh surface identified by STM.

Fig. 6 shows the C 1s core-level spectra recorded from the "pure carbon nanomesh surface" at two emission angles of 90° and 40° using a photon energy of 350 eV. The raw data are shown by black dots. The results of the curve-fitting of the C 1s spectra are also shown in Fig. 6. For the surface sensitive mode at an emission angle of 40°, the C 1s spectrum is dominant by a broad surface-related structure, which contains at least two components: a strong component (S_1) located at

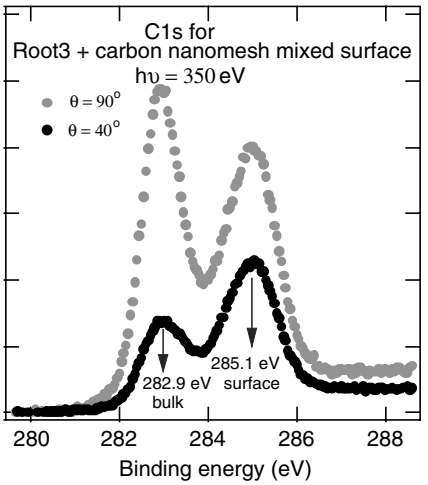

Fig. 5. C 1s core-level spectra recorded from the "$\sqrt{3} \times \sqrt{3}R30^\circ$ + carbon nanomesh mixed surface" using a photon energy of 350 eV and emission angles of 40° and 90°.

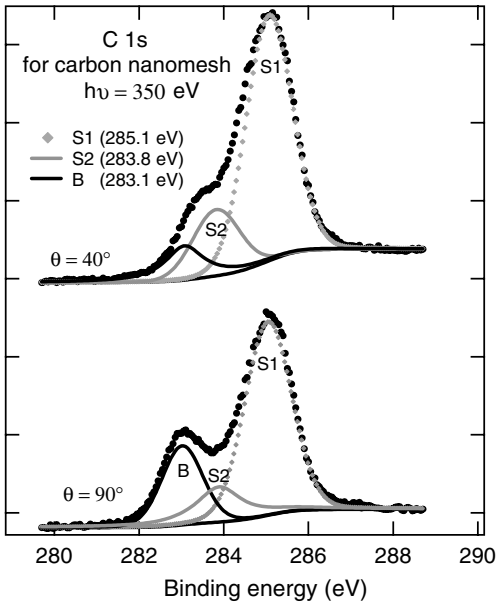

Fig. 6. C 1s core-level spectra recorded from the "pure carbon nanomesh surface" using a photon energy of 350 eV and emission angles of (a) 40° and (b) 90°.

285.1 eV and a weaker one (S_2) at 283.8 eV. The ratio of the peak area intensities for the components S_2 and S_1 (I_{S2}/I_{S1}) is about 0.35. For the less surface sensitive mode at an emission angle of 90°, the bulk-related component (B) at 282.9 eV is enhanced. Simple attenuation models were used to estimate the thickness of the C species on the carbon nanomesh surface using the C 1s spectrum data of the carbon nanomesh and the well-developed $\sqrt{3}\times\sqrt{3}R30°$ surfaces recorded at an emission angle of 90° and phonon energy of 350 eV. In our previous experiments of Co nanocluster formation on the carbon nanomesh, we observed that Co species do not react with the underlying SiC to form cobalt silicides during annealing [11,12]. This suggests that the centers of the carbon nanomesh are also covered by carbon layers that prevent Co reaction to form cobalt silicides, as reported on 6H–SiC(0 0 0 1)-$\sqrt{3}\times\sqrt{3}R30°$ and 3×3 surfaces [34,35]. Therefore, we first consider the model where the carbon nanomesh top layer lies above one or a few complete carbon layers as shown in Fig. 7(a). The thickness of the carbon nanomesh is estimated using Eq. (1) [36]:

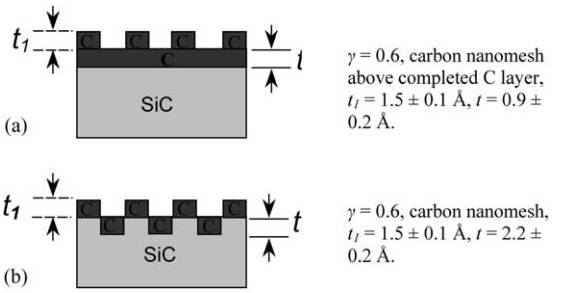

Fig. 7. Schematic models of the carbon nanomesh surface: the light grey region represents bulk SiC and the dark grey region represents the carbon nanomesh structure and carbon layer: (a) the carbon nanomesh top layer rests above a completed carbon thin film, and (b) the centers of carbon nanomesh are occupied by carbon species.

$$\frac{I_{\mathrm{SiC}}^{\mathrm{nanomesh}}}{I_{\mathrm{SiC}}^{\mathrm{Root3}}} = \frac{I_{\mathrm{SiC}}^{\infty}\{\gamma\exp[-(t+t_1)/\lambda]+(1-\gamma)\exp(-t/\lambda)\}}{I_{\mathrm{SiC}}^{\infty}} = \gamma\exp[-(t+t_1)/\lambda]+(1-\gamma)\exp(-t/\lambda), \quad (1)$$

where $I_{\mathrm{SiC}}^{\mathrm{nanomesh}}$ is the normalized peak area intensity of the bulk-related component (component B located at 282.9 eV) in the C 1s spectrum of the pure nanomesh surface, $I_{\mathrm{SiC}}^{\mathrm{Root3}}$ is the normalized peak area intensity of the bulk-related C 1s peak of the well-developed $\sqrt{3}\times\sqrt{3}R30°$ reconstruction, $I_{\mathrm{SiC}}^{\infty}$ is normalized peak area intensity of the C 1s peak of the clean SiC substrate, γ is the coverage of the carbon nanomesh, t_1 is the thickness of the carbon nanomesh, t is the thickness of the completed carbon layers, and λ is the electron escape depth or attenuation length with kinetic energy of E_{k} in the carbon nanomesh. The ratio of $\frac{I_{\mathrm{SiC}}^{\mathrm{nanomesh}}}{I_{\mathrm{SiC}}^{\mathrm{Root3}}}$ is 0.64 as determined from PES data. The electron escape depth (λ) of 4.0 Å at kinetic energy about 60 eV ($E_{\mathrm{k}} = h\nu - E_{\mathrm{B}} - \varphi$) is used for the calculation [31]. Based on this model, γ is estimated from STM images to be 0.6 (Fig. 1). In order to simplify the calculation, the thickness (t_1) of the carbon nanomesh was estimated from the STM results, where $t_1 = 1.5 \pm 0.1$ Å. From Eq. (1), $t = 0.9 \pm 0.2$ Å, which is significantly thinner than a single layer of carbon atoms. Hence, this model is unsatisfactory as it overestimates the amount of surface carbon.

In the next model, we consider the situation where the carbon nanomesh lies above an uncompleted carbon layer where only the centers of the nanomesh are terminated by carbon species as shown in Fig. 7(b). The thickness of the carbon nanomesh is estimated using Eq. (2) [36]:

$$\frac{I_{\mathrm{SiC}}^{\mathrm{nanomesh}}}{I_{\mathrm{SiC}}^{\mathrm{Root3}}} = \frac{I_{\mathrm{SiC}}^{\infty}[\gamma \exp(-t_1/\lambda) + (1-\gamma)\exp(-t/\lambda)]}{I_{\mathrm{SiC}}^{\infty}} = \gamma \exp(-t_1/\lambda) + (1-\gamma)\exp(-t/\lambda), \quad (2)$$

where t_1 is the thickness of the carbon nanomesh, t is the thickness of the underlying carbon layer, and $\gamma = 0.6$. We assume the thickness of the carbon nanomesh t_1 to be 1.5 ± 0.1 Å in order to estimate t. From Eq. (2), $t = 2.2 \pm 0.2$ Å. Due to the finite STM tip effect, the thickness (t_1) of the carbon nanomesh is probably slightly underestimated, and the estimated thickness t of the underlying carbon layer is probably overestimated. Since both t_1 (1.5 ± 0.1 Å) and t (2.2 ± 0.2 Å) are close to the thickness of a monolayer of carbon atoms, we assume that both the carbon nanomesh and underlying carbon layer are one-atom-layer thick with equal thickness of t. Therefore, we propose a model to describe the structure of the carbon nanomesh surface whereby isolated carbon islands one atomic layer thick assemble to form the nanomesh structure; while the center of the honeycombs are also covered by one-atom-layer thick carbon islands as shown in Fig. 7(b). Since the whole surface is covered by these carbon island domains, they can act as a barrier layer to prevent Co nanoclusters from reacting with the underlayer Si atoms to form cobalt silicide during the cluster formation and annealing process [11,12].

To understand the atomic structure of the carbon nanomesh surface, we carried out first-principles total energy calculations. Pseudopotential density-functional theory (DFT) [37,38] calculations were carried out using the Vienna ab initio simulation package (VASP) [39–41] which iteratively solves the Kohn–Sham equation in a plane wave basis set. Here, the local-density approximation (LDA) [38] was employed for exchange and correlation energy, and Vanderbilt-type ultrasoft pseudopotentials [42] supplied by Kresse and Hafner [43] were used for all the three elements. A cutoff energy of 286.6 eV was used in all calculations. Based on the synchrotron PES results (Fig. 7(b)), we have suggested that the whole surface of the nanomesh template was covered by tiny carbon islands, which self-organized to form the honeycomb structures. As such we proposed models that contain three SiC bilayers covered by isolated carbon domains that represent the nanomesh structure. A large number of models were considered and calculated, and here we present the 6×6 supercell model that best fits both the STM and PES results. Fig. 8(c) and (d) show the top and side views respectively of the supercell model. The bottom C layer is saturated by partially

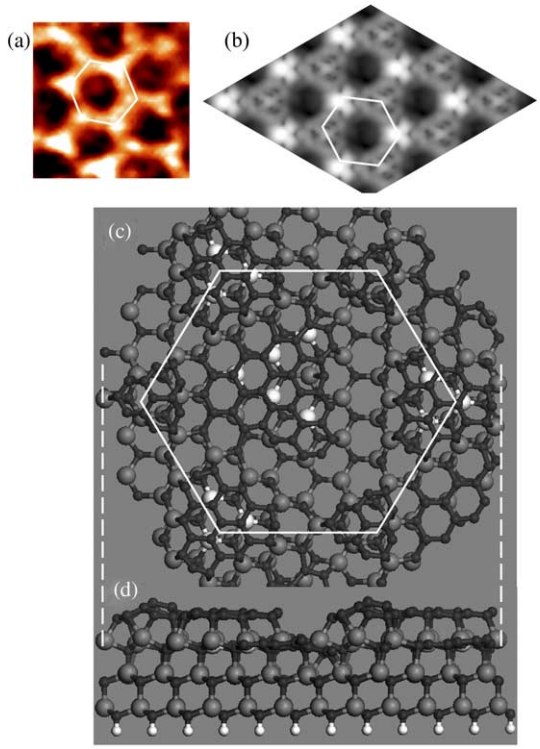

Fig. 8. (a) 55×55 Å^2 filled state STM image of the carbon nanomesh surface, $V_T = 1.5$ V, $I = 0.2$ nA, (b) corresponding calculated STM image at bias of $V_T = 1.5$ V, (c) top view and (d) side view of the 6×6 model, the small dark spheres represent C atoms, big grey spheres for Si atoms, big white spheres for the Si atoms with dangling bonds, and small white spheres for H atoms. The white hexagon highlights the honeycomb unit cell in the experimental and calculated STM images, and in the 6×6 supercell model.

charged hydrogen atoms [44]. Adjacent slabs are separated by a vacuum layer of about 10 Å. The structure optimizations were converged within 10 meV/Å for the total force per atom. To compare with experimental STM images, we calculated constant-current STM images at tip bias of 1.5 V using the Tersoff–Hamann approach [45] as shown in Fig. 8(b). The calculated STM image (Fig. 8(b)) is in qualitative agreement with experiment observations (Fig. 8(a)). Since the 6×6 supercells are the dominant structure on the carbon nanomesh surface, we only calculated the 6×6 superstructures for comparison with experiment results. Further studies on the other structures will be reported separately.

As shown in the 6×6 model, there are basically two kinds of surface-related carbon atoms that make up the carbon nanomesh structures:

(1) Carbon atoms (A) that bond to one underlying Si atom. The binding energy of these C atoms is expected to be higher than that of the bulk SiC-related C atoms (282.9 eV, bonded to four Si atoms), but lower than that of the C atoms from graphite (284.4 eV). Since the S_2 peak is located at 283.8 eV, we attribute the S_2 peak to the A atoms.
(2) Carbon atoms (B) that lie above the SiC surface without formation of Si–C bonds. These B atoms form the 6 C-rings or graphene-like structures with delocalized π-electrons to minimize the total energy. We postulate that the S_1 peak arises from photoemissions from these B atoms. From the model, the B atoms are located above Si atoms that possess one unsaturated bond or dangling bond as highlighted by big white spheres in Fig. 8(c). In order to lower the total energy of the system, the B atoms may partially share their delocalized π-electrons with the unsaturated bond on the Si atoms [46], hence causing the B atoms to be slightly positive charged compared to graphite. As such, the S_1 peak is expected to be at higher binding energy compared to graphite (284.4 eV), consistent with our measured S_1 binding energy of 285.1 eV.

Forbeaux, et al., observed some fingerprints of graphite with π* and σ* bands even for the "$6\sqrt{3}\times6\sqrt{3}R30^\circ$ and $\sqrt{3}\times\sqrt{3}R30^\circ$ mixed surface" (equivalent to the "$\sqrt{3}\times\sqrt{3}R30^\circ$ + carbon nanomesh mixed surface" in this paper) from angular-resolved inverse photoemission spectroscopy (KRIPES), and suggested that a graphite layer forms on SiC surface at this stage [25]. However, both Johansson's high resolution PES results [19] and our synchrotron PES data reveal the formation of a graphite layer at a higher temperature than that required for the well-developed carbon nanomesh surface. The contradiction of the advance appearance of graphite fingerprints in KRIPES experiments can be explained by the model proposed in Fig. 8. This nanomesh surface comprises tiny carbon islands with delocalized π-electrons, which can be considered as tiny graphite-like islands. We also suggest that the "carbon nanomesh and $\sqrt{3}\times\sqrt{3}R30^\circ$ mixed surface" was mixed with these tiny graphite islands and $\sqrt{3}\times\sqrt{3}R30^\circ$ reconstruction at different surface regions as shown in Fig. 3(a). Therefore, the observed graphite fingerprints of π* and σ* bands on the "carbon nanomesh and $\sqrt{3}\times\sqrt{3}R30^\circ$ mixed surface" in the KRIPES experiments may be due to these tiny graphite islands. After annealing at temperatures higher than that required for the well-developed carbon nanomesh surface, crystalline graphite multilayers were formed on top of the SiC surface [13–19,25]. Due to the very weak van der Waals interaction between crystalline graphite multilayers and SiC substrate [25], there is no charge transfer between them and hence, these crystalline graphite multilayers show the same binding energy (284.4 eV) as that of HOPG (Fig. 4). Moreover, those tiny graphite islands will be progressively buried under the growing graphite multilayers after annealing at higher temperature. As such, the C 1s peak intensity from those tiny graphite islands progressively vanishes as shown in Fig. 4.

4. Conclusion

We have investigated the atomic structure of the carbon nanomesh formed on 6H–SiC(0001) using combined in situ STM, LEED, synchrotron

photoemission experiments and DFT theoretical calculations. We postulate that the formation of the carbon nanomesh is due to the self-organization of carbon atoms on the surface accompanying the evaporation of silicon atoms from the bulk at around 1100 °C. DFT calculations are used to identify possible surface structures that yield similar simulated STM images. Two surface-related C 1s PES components for the carbon nanomesh surface have been identified at binding energies of 285.1 eV (S_1) and 283.8 eV (S_2), respectively. The S_2 peak is attributed to carbon atoms that bond to one underlying Si atom, and the S_1 peak to carbon atoms that lie above the SiC surface without Si–C bond formation. After prolonged annealing, more carbon atoms will accumulate on the surface to enlarge the pore size as well as the apparent height of the carbon nanomesh. Annealing at higher temperature leads to the formation of crystalline graphitic layers, consistent with previous reports of the observation of graphite layers on the top surface [13–17].

Acknowledgements

W. Chen and L. Liu acknowledge the support from National University of Singapore under the grant of R-144-000-107-112.

References

[1] H. Brune, M. Giovannini, K. Bromann, K. Kern, Nature 394 (1998) 451.
[2] K.H. Wu, Y. Fujikawa, T. Nagao, Y. Hasegawa, K.S. Nakayama, Q.K. Xue, E.G. Wang, T. Briere, V. Kumar, Y. Kawazoe, S.B. Zhang, T. Sakurai, Phys. Rev. Lett. 91 (2003) 126101.
[3] J.L. Li, J.F. Jia, X.J. Liang, X. Liu, J.Z. Wang, Q.K. Xue, Z.Q. Li, J.S. Tse, Z.Y. Zhang, S.B. Zhang, Phys. Rev. Lett. 88 (2002) 066101.
[4] F. Rosei, J. Phys. Condens. Matter 16 (2004) S1373.
[5] F. Rosei, M. Schunack, P. Jiang, A. Gourdon, E. Laegsgaard, I. Stensgaard, C. Joachim, F. Besenbacher, Science 296 (2002) 328.
[6] R. Otero, Y. Naitoh, F. Rosei, P. Jiang, P. Thostrup, A. Gourdon, E. Laegsgaard, I. Stensgaard, C. Joachim, F. Besenbacher, Angew. Chem. Int. Ed. 43 (2004) 2092.
[7] J. Weckesser, A. De Vita, J.V. Barth, C. Cai, K. Kern, Phys. Rev. Lett. 87 (2001) 096101.
[8] H. Spillmann, A. Dmitriev, N. Lin, P. Messina, J.V. Barth, K. Kern, J. Am. Chem. Soc. 125 (2003) 10725.
[9] J.A. Theobald, N.S. Oxtoby, M.A. Phillips, N.R. Champness, P.H. Beton, Nature 424 (2003) 1029.
[10] M. Corso, W. Auwärter, M. Muntwiler, A. Tamai, T. Greber, J. Osterwalder, Science 303 (2004) 217.
[11] W. Chen, K.P. Loh, H. Xu, A.T.S. Wee, Appl. Phys. Lett. 84 (2004) 281.
[12] W. Chen, K.P. Loh, H. Xu, A.T.S. Wee, Langmuir 20 (2004) 10779.
[13] L. Li, I.S.T. Tsong, Surf. Sci. 351 (1996) 141.
[14] H. Tsai, C.S. Chang, John D. Dow, I.S.T. Tsong, Phys. Rev. B 45 (1992) 1327.
[15] C.S. Chang, I.S.T. Tsong, Y.C. Wang, Surf. Sci. 256 (1991) 354.
[16] J.E. Northrup, J. Neugebauer, Phys. Rev. B 52 (1995) R17001.
[17] V. van Elsbergen, T.U. Kampen, W. Mönch, Surf. Sci. 365 (1996) 443.
[18] F. Owman, P. Måtrensson, Surf. Sci. 369 (1996) 126.
[19] L.I. Johansson, F. Owman, P. Mårtensson, Phys. Rev. B 53 (1996) 13793.
[20] P. Mårtensson, F. Owman, L.I. Johansson, Phys. Status Solidi B 202 (1997) 501.
[21] L.I. Johansson, F. Owman, P. Mårtensson, Surf. Sci. 360 (1996) L483.
[22] L. Simon, J.L. Bischoff, L. Kubler, Phys. Rev. B 60 (1999) 11653.
[23] U. Starke, J. Schardt, M. Franke, Appl. Phys. A 65 (1997) 587.
[24] U. Starke, M. Franke, J. Bernhardt, J. Schardt, K. Reuter, K. Heinz, Mater. Sci. Forum 264 (1998) 321.
[25] I. Forbeaux, J.-M. Themlin, J.-M. Debever, Phys. Rev. B 58 (1998) 16396.
[26] M.A. Kulakov, H. Hoster, G. Henn, B. Bullemer, Mater. Sci. Eng. B 46 (1997) 227.
[27] Y. Hisada, K. Hayashi, K. Kato, T. Aoyama, S. Mukainakano, A. Ichimiya, Jpn. J. Appl. Phys. 40 (4A) (2001) 2211.
[28] W. Chen, X.N. Xie, H. Xu, A.T.S. Wee, K.P. Loh, J. Phys. Chem. B 107 (2003) 11597.
[29] H.Y. Lin, Y.P. Chiu, L.W. Huang, Y.W. Chen, T.Y. Fu, C.S. Chang, T.T. Tsong, Phys. Rev. Lett. 94 (2005) 136101.
[30] A.J. Bommel, J.E. Crombeen, A. van Tooren, Surf. Sci. 48 (1975) 463.
[31] C. J. Powell, A. Jablonski, NIST Electron Effective-Attenuation-Length Database, Version 1.0, 2001.
[32] S. Helveg, C. Lopez-Cartes, J. Sehested, P.L. Hansen, B.S. Clausen, J.R. Rostrup-Nielsen, F. Abild-Pedersen, J.K. Norskov, Nature 427 (2004) 426.
[33] R. Rosei, M. De Crescenzi, F. Sette, C. Quaresima, A. Savoia, P. Perfetti, Phys. Rev. B 28 (1983) 1161.
[34] W. Platow, D.K. Wood, K.M. Tracy, J.E. Burnette, R.J. Nemanich, D.E. Sayers, Phys. Rev. B 63 (2001) 115312.
[35] W. Platow, R.J. Nemanich, D.E. Sayers, J.D. Hartman, R.F. Davis, J. Appl. Phys. 90 (2001) 5924.
[36] C.S. Fadley, Prog. Surf. Sci. 16 (1984) 275.

[37] P. Hohenberg, W. Kohn, Phys. Rev. 136 (1964) B864.
[38] W. Kohn, L.J. Sham, Phys. Rev. 140 (1965) A1133.
[39] G. Kresse, J. Hafner, Phys. Rev. B 47 (1993) 558.
[40] G. Kresse, J. Furthmüller, Phys. Rev. B 54 (1996) 11169.
[41] G. Kresse, J. Furthmüller, Comput. Mater. Sci. 6 (1996) 15.
[42] D. Vanderbilt, Phys. Rev. B 41 (1990) 7892.
[43] G. Kresse, J. Hafner, J. Phys. Condens. Matter 6 (1994) 8245.
[44] K. Shiraishi, J. Phys. Soc. Jpn. 59 (1990) 3455.
[45] J. Tersoff, D.R. Hamann, Phys. Rev. B 31 (1985) 805.
[46] Y. Taguchi, M. Fujisawa, M. Nishijima, Chem. Phys. Lett. 178 (1991) 363.
[47] X.J. Yu, O. Wilhelmi, H.O. Moser, S.V. Vidyarai, X.Y. Gao, A.T.S. Wee, T. Nyunt, H. Qian, H. Zheng, J. Electron Spectrosc. Relat. Phenom. 144–147 (2005) 1031.